**Proceedings of the 8th International Pipeline Conference**
**IPC 2010**
**September 27 – October 1, 2010, Calgary, Alberta, Canada**

**IPC 2010-31316**

# A MATHEMATICAL MODEL DEVELOPED TO PREDICT THE CHEMISTRY AND CORROSION RATE IN A COATING DISBONDED REGION OF VARIABLE GAP

**Fengmei Song**

Mechanical Engineering
Southwest Research Institute
San Antonio, TX, USA 78238

## ABSTRACT

A model is developed to predict the chemistry, corrosion potential and rate of pipeline steels in a coating disbonded region. The gap of the disbonded region is assumed to vary with distance from the holiday. The effect of this gap variation on the chemistry and corrosion rate in the coating disbonded region is not well understood and investigated in this study through modeling. The preliminary model results suggest that overall, the variation of the disbondment gap with distance has an insignificant effect on the pH, corrosion potential and rate in the disbonded region. This may be explained as that unlike some conventional crevice corrosion often associated with a large cathode-to-anode area ratio, the area ratio here is rather relatively small and the pH commonly falls in the neutral or alkaline range. Within this pH range, even if the pH varies within a few units across the crevice length, the variation of the crevice corrosion rate is not significant. In this paper, the fundamental principles used for the model, some key model results and practical implications of the results are reported and discussed.

## INTRODUCTION

Significant research has been performed in the past to understand the mechanisms of external corrosion of underground pipelines under disbonded coatings with or without a holiday[1-25]. The crevice has generally been made to have a constant gap in laboratory tests[4,17-24] or in mathematically modeling[5-13]. In reality, this gap rarely is a constant. It can vary in the longitudinal direction of the crevice and it can vary over time when the metal dissolves into solution (the corrosion rate varies from the holiday down into the disbonded region). In addition, ionic current or oxygen diffusion through a permeable disbonded coating is often not included in such crevice corrosion tests, although models were reported which consider the effect of current or oxygen permeation through the coating[7,13,26-27]. A goal of this work is to understand from a fundamental perspective, by mathematical modeling, the effect of variable crevice gap and the permeability of a coating to CP and/or oxygen on the crevice corrosion rate.

The crevice geometries to be studied in this work are shown in Figure 1. The model simulation focuses on one dimensional (1D) in the "x" direction . $O_2$ transport in two dimensions (2D) is simplified as semi-2D, similar to what was done elsewhere[8,13,27]. Direct 1D simulation for $O_2$ diffusion in the crevice is challenging because $O_2$ has a high concentration and low gradient near the coating and a low concentration and high gradient near the steel surface. To simplify this 2D transport of $O_2$, a parabolic relation of $O_2$ concentration vs. y across the gap is assumed for each point along "x". This assumption was proven to be sufficiently accurate[12] that the $O_2$ concentration profile along "x" obtained under this assumption coincides with that computed from a full 2D model with this parabolic relation imposed only at the holiday mouth (z=0).

The crevice solution used in this modeling is a dilute aerated sodium chloride solution simulating soil ground water. The solution is assumed to be saturated by ferrous hydroxide which is only sparsely soluble in water. The effect of the homogeneous ferrous ion oxidation on the crevice corrosion rate is neglected due to justifications given elsewhere[28].

The general mass transport equations to describe the pipeline crevice corrosion process are derived first, followed by the equations of corrosion reactions in the presence of $O_2$.

 Copyright © 2010 by ASME

## THE MATHEMATICAL MODEL

*The Model Geometry*

The crevice geometries used in the model of this work are shown in Figure 1, formed due to a coating disbonded from the pipe surface and the holiday located at the left edge of the disbonded region. For the crevice geometry shown in Figure 1a, the temporal and spatial variation of the crevice chemistry and corrosion potential and rate were modeled extensively by the author and coworkers.[13] Corrosion of a crevice with its gap varying with distance from the holiday, as shown in Figure 1b and 1c, has not been investigated, although it is expected it may have an effect on the evolution of crevice chemistry and corrosion.

Figure 1b is an extreme case where the gap changes abruptly at $\frac{x}{\delta_{s0}} = 5$, 6, 15 and 100; x is arbitrary distance from the holiday and $\delta_{s0}$ is gap at the holiday edge. It is expected that such a sharp variation of gap would yield a more significant impact on the crevice corrosion than if the gap varies more gradually as shown in Figure 1c or is constant as shown in Figure 1a.

The crevice gap variation in Figure 1b may expressed by:

$$\frac{\delta_s}{\delta_{s0}} = 1 \qquad \text{when } \frac{x}{\delta_{s0}} = \text{0-5, 6-15, 100-200, and}$$

$$\frac{\delta_s}{\delta_{s0}} = \frac{1}{4} \qquad \text{when } \frac{x}{\delta_{s0}} = \text{5-6, 15-100,}$$

where $\delta_s$ is gap at variable distance x in the crevice. The above discrete equations may be combined and written as:

$$\frac{\delta_s}{\delta_{s0}} = 1 + \theta_1[-\tfrac{3}{4}(\tfrac{x}{\delta_{s0}} > 5) + \tfrac{3}{4}(\tfrac{x}{\delta_{s0}} > 6) - \tfrac{3}{4}(\tfrac{x}{\delta_{s0}} > 15) + \tfrac{3}{4}(\tfrac{x}{\delta_{s0}} > 100)] \tag{1}$$

where $\theta_1$ serves as a switch in the computer code. $\theta_1$=0 represents a constant crevice gap, and $\theta_1$=1 represents a variable crevice gap as shown in Figure 1b.

The gap variation for Figure 1c follows:

$$\frac{\delta_s}{\delta_{s0}} = 1 \qquad \text{when } \frac{x}{\delta_{s0}} = \text{0-5, 6-15, 100-200,}$$

$$\frac{\delta_s}{\delta_{s0}} = \frac{1}{4} \qquad \text{when } \frac{x}{\delta_{s0}} = \text{5-6, 30-70}$$

$$\frac{\delta_s}{\delta_{s0}} = 1 - \frac{3}{4} \cdot \frac{\text{x-15}}{15} \quad \text{when } \frac{x}{\delta_{s0}} = \text{15-30, and}$$

$$\frac{\delta_s}{\delta_{s0}} = \frac{1}{4} + \frac{3}{4} \cdot \frac{\text{x-70}}{30} \quad \text{when } \frac{x}{\delta_{s0}} = \text{70-100, or}$$

The above discrete equations may be combined to yield:

$$\frac{\delta_s}{\delta_{s0}} = 1 + \theta_2[-\tfrac{3}{4}(\tfrac{x}{\delta_{s0}} > 5) + \tfrac{3}{4}(\tfrac{x}{\delta_{s0}} > 6) - \tfrac{3}{4} \cdot \frac{\frac{x}{\delta_{s0}} - 15}{15}(\tfrac{x}{\delta_{s0}} > 15)(\tfrac{x}{\delta_{s0}} \le 30) - \tfrac{3}{4}(\tfrac{x}{\delta_{s0}} > 30) + \tfrac{3}{4} \cdot \frac{\frac{x}{\delta_{s0}} - 70}{30}(\tfrac{x}{\delta_{s0}} > 70)(\tfrac{x}{\delta_{s0}} \le 100) + \tfrac{3}{4}(\tfrac{x}{\delta_{s0}} > 100)] \tag{2}$$

Like $\theta_1$, $\theta_2$ also serves as a switch. $\theta_2$=0 represents a constant crevice gap. $\theta_2$=1 represents a variable crevice gap as shown in Figure 1c. The gap varies with "x" linearly in $\frac{x}{\delta_{s0}} = 15 \sim 30$ and in $\frac{x}{\delta_{s0}} = 70 \sim 100$.

The gap is designed to have abrupt variations at $x/\delta_{s0}$= 5 and 6 because it was learned in the past[5-13] that the change of variables would occur most strongly within the first 10 gaps from the mouth. Abrupt or gradual changes of gap are designed to also occur in intermediate ($x/\delta_{s0}$= 15) and longer ($x/\delta_{s0}$= 100) distances to understand how gap changes at these locations would have an effect on the corrosion (relative to the corrosion in a crevice of constant gap).

*Model Conditions*

The following species are present in the solution: $\underline{Na^+}$ --(1), $\underline{Cl^-}$ --(2), $Fe^{2+}$ --(3), $\underline{H^+}$ --(4), $OH^-$ --(5), $Fe(OH)^+$ --(6), $\underline{O_2}$ --(7), $\underline{H_2(aq)}$ --(8), $\underline{Fe(OH)_2}$ --(9) and $\underline{H_2O}$ --(10). The species underlined are defined as the primary species. Their concentrations can either be approximated, or known such as species 8-10. The concentrations of the secondary species, or species 3, 5 and 6, can be determined from the concentrations of the primary species through their equilibrium equations given in Appendix A.

It is assumed that the coating disbonds before a holiday is formed in the coating. Water vapor and oxygen can permeate through the coating to cause the pipe corrosion underneath. Depending on the type, thickness and degree of deterioration of the coating, the permeability of oxygen through the coating varies. Two conditions of a coating are considered by its permeability to oxygen and/or current: (1) the coating is impermeable to either oxygen or CP, (2) the coating is permeability to either or both of oxygen or/and CP. The permeability is determined by the effective area of the coating that allows the penetration of oxygen or/and CP through the disbonded coating.

Regardless of the permeability of the coating to oxygen and/or CP, when water vapor permeates through the disbonded coating, corrosion may start and a steady state condition may be established. The chemistry in the crevice can be different from that in soil and can be saturated by the sparsely soluble ferrous hydroxide. In the presence of oxygen, the formation of ferric oxide suspension in solution may reduce the corrosion rate by consuming oxygen (which otherwise may contribute to corrosion). On the other hand, the formation of iron oxide may also enhance localized pitting when this oxide is adherent to the steel surface. Although the potential effect of ferric oxide


Copyright © 2010 by ASME

formation on the crevice corrosion rate was briefly treated in earlier work[27-28], the effect due to localized pitting in the crevice as a more complex issue has not be dealt with in the past and it will not be a part of the study here.

When the pipe surface contains contaminant salts before coating, it is possible that the soluble species may dissolve in the solution in the disbonded region. The model considers a dilute NaCl solution in the disbonded region than in the bulk soil. This disbonded chemistry may have been stable before the disbonded coating is breached and a holiday created. When that happens, the direct transport of oxygen and solution species (or CP) through the holiday solution will modify the conditions in the disbonded region. For this work, it is assumed that the stable solution in the disbonded region is more dilute than in the bulk soil before the holiday is created.

The effect of variable crevice gap vs. distance and time, and/or the permeation of oxygen and/or CP through the crevice holiday and/or the disbonded coating are investigated. However, for the purpose of this paper, only the variation of gap vs. distance is reported. The primary goal is to understand the temporal and spatial variation of crevice chemistry and corrosion rate.

The scenario to be modeled may also apply to a condition where the coating holiday was created prior to formation of a disbonded region. Then, it is possible that the entire disbonded region and the holiday may in some point of time experience a dry-out with complete loss of CP, and later, the soil becomes wet and CP starts to function again. In this case, the solution in the disbonded region may or may not be more dilute than in the soil ground water.

Aside of all the practical significance for the cases being investigated, this model is also significant from a fundamental perspective in that it solves challenging problems that have not been explored before.

In this work, the 3D geometry of a crevice is first simplified into 2D by consideration of the relatively much larger crevice width (dimension not shown in Figure 1) to gap. This 2D geometry can be further simplified into 1D or more properly called semi-2D. A direct simplification of 2D into 1D does not properly account for the complex oxygen diffusion in the crevice.

A special treatment of oxygen transport in a crevice has been described extensively in earlier work[8,13,27], although this treatment to include $O_2$ diffusion through a disbonded coating appears cumbersome in the way previously presented, it is reorganized and shown in Appendix B.

*Model Governing Equations*

By considering all the possible reversible and irreversible chemical and electrochemical reactions in the crevice corrosion system, by use of the equilibrium relations for reversible reactions given in Appendix A, the mass transport equation for each primary species and the equation of electroneutrality can be written below:

$$\frac{\partial(\delta_s c_1)}{\partial t} + \frac{\partial}{\partial x}(\delta_s N_{1x}) + N_{1yc} = 0 \tag{3}$$

$$\frac{\partial(\delta_s c_2)}{\partial t} + \frac{\partial}{\partial x}(\delta_s N_{2x}) + N_{2yc} = 0 \tag{4}$$

$$\begin{aligned}&\frac{\partial}{\partial t}(\delta_s \sum_3^6 z_j c_j) + \frac{\partial}{\partial x}(\delta_s \sum_3^6 z_j N_{jx}) + \sum_3^6 z_j N_{jyc} \\ &- (2r^e_{Fe} + r^e_H + r^e_{H_2O} + 4r^e_{O_2}) = 0\end{aligned} \tag{5}$$

$$\sum_1^6 z_j c_j = 0 \tag{6}$$

$$\begin{aligned}&\frac{\partial(\delta_s \bar{c}_7)}{\partial t} + \frac{\partial}{\partial x}(\delta_s N_{7x}) + N_{7yc} \\ &= \frac{2D_{O_2}[3m(\pi+2)c_7^0 - 6(m+\pi+m\pi)\bar{c}_7]}{\delta_s(4m+12+\pi m+4\pi)}\end{aligned} \tag{7}$$

where t is time, $z_j$, $c_j$, and $N_j$ are respectively the charge, concentration and flux of the $j^{th}$ species. $\delta_s$ is the boundary layer thickness. Subscribe "x" means "x" direction and subscript "yc" means in "y" direction across the coating. $r^e$ represents the electrochemical (anodic or cathodic) reaction rate, with the key element involving the reaction shown in the subscript of the "r" term. These electrochemical reactions and the "r" expressions are given in Appendix A and will also be presented in the main text later.

In Equation (7), $\bar{c}_7$ and $c_7^0$ are respectively $O_2$ concentration averaged across the crevice gap and that in bulk soil, $D_{O_2}$ is oxygen diffusion coefficient in solution, m and $\pi$ are terms that are defined in Appendix B. $m = \frac{D_{O_2c}/\delta_c}{D_{O_2}/\delta_s}$, a ratio of the coating permeability to that of the solution layer; $D_{O2c}$ and $\delta_c$ are respectively $O_2$ diffusivity in coating and the coating thickness. Both m and $\pi$ will be described later.

In the above equations, the flux of the $j^{th}$ species in the crevice solution in the longitudinal direction $N_{jx}$ may be written as:

$$N_{jx} = -D_j \frac{\partial c_j}{\partial x} - \frac{z_j D_j F}{RT} c_j \frac{\partial \varphi}{\partial x} \tag{8}$$

where the 1st and 2nd terms on the right hand to the equal sign are the diffusion and migration components of the $j^{th}$ species in the "x" direction. F, R and T are respectively Faraday's constant, universal gas constant and temperature in K. $\varphi$ is electrostatic potential of the solution.

The flux in the y direction shown by $N_{jyc}$ represents the transport of $j^{th}$ species through the coating and it is one component of the ionic current flow passing through the disbonded coating. For simplicity, a linear gradient of the concentration and the electrostatic potential of the solution is assumed across the coating and thus, $N_{jyc}$ has of the form:


Copyright © 2010 by ASME

$$N_{jyc} = \theta_3(-D_j \frac{c_{j0}-c_j}{\delta_c} - \frac{z_j D_j F}{RT}\frac{c_{j0}+c_j}{2}\frac{\varphi_0-\varphi}{\delta_c}) \quad (9)$$

and, for $O_2$,

$$N_{7yc} = -D_{O_2c}\frac{c_{j0}-c_j}{\delta_c} \quad (10)$$

Like $\theta_1$ and $\theta_2$ in Equations (1) and (2) respectively, $\theta_3$ serves as a switch in the computer code. $\theta_3 = 0$ represents no CP penetration through the coating and $\theta_3 = 1$ represents CP penetration through the coating. In the last term on the right hand of Equation (9), the concentration in the coating is approximated by the average across the coating, or $0.5(c_j+c_{j0})$.

The derivation of Equation (7) has been given in Appendix B. The term on the right hand to the equal sign has already included oxygen transport through the coating, embedded in the "m" parameter. When $D_{O2c}$ is set to be zero, m=0, and thus, the $O_2$ diffusion rate through the coating is automatically eliminated.

When the change of the crevice gap with time is considered to account for the continuous dissolution of steel into the solution, the following moving boundary condition must be included following Faraday's law,

$$\frac{\partial \delta_s}{\partial t} = \theta_4 \alpha r^e_{Fe} \quad (11)$$

where $\alpha$ is unit conversion factor with $\alpha = \frac{z_{Fe}F\rho_{Fe}}{M_{Fe}}$ where M is atomic weight of steel ($M_{Fe}$), $z_{Fe}$ is valency of solvated species or $Fe^{2+}$ here, and $\rho_{Fe}$ is the density of steel. In Equation (11), $\theta_4$ serves as a switch in the computer code. $\theta_4 = 0$ represents time independent crevice gap (or the change of gap by metal dissolution is neglected) and $\theta_4 = 1$ represents the crevice gap varies as the steel surface dissolves into solution.

Since Equation (11) is an ordinary differential equation, it requires only the initial condition of the gap, although the gap may vary with x, distance from the holiday. No boundary condition is required.

Equation (6) may alternatively be replaced by:

$$\frac{\partial}{\partial x}(\delta_s \sum_1^6 z_j N_{jx}) + \sum_1^6 z_j N_{jyc} - (2r^e_{Fe} + r^e_H + r^e_{H_2O} + 4r^e_{O_2}) = 0 \quad (12)$$

The electrochemical reaction rates can be converted from the corresponding current density following Faraday's law:

$$r^e_l = \frac{i_l}{n_l F} \quad (13)$$

where l represents Fe, $H^+$, $H_2O$, and $O_2$. n is the number of electrons of charge transfer in an elemental half cell reaction.

The corrosion or iron oxidation current density ($i_{Fe}$) is assumed to follow the Tafel equation given below:

$$i_{Fe} = i^0_{Feref} 10^{\frac{E-E^{Eqref}_{Fe}}{b_{Fea}}} \quad (14)$$

where E is the electrode/pipe potential with respect to an arbitrary reference electrode, which is in this work consistently referred to as the saturated $Cu/CuSO_4$ electrode (CSE). "ref" in either subscript or superscript is referred to as a reference condition whereby the corresponding exchange current density $i^0$, concentration $c_j$ (j=3, 4, 5, 14) and equilibrium potential $E^{Eq}$ are known. "b" is Tafel slope.

For reductions of hydrogen ion and water, their Tafel equations are respectively:

$$i_H = -i^0{}_{Href}\frac{c_4}{c_{4ref}} 10^{\frac{-(E-E^{Eqref}_H)}{b_H}} \quad (15)$$

and

$$i_{H_2O} = -i^0{}_{H_2Oref} 10^{\frac{-(E-E^{Eqref}_{H_2O})}{b_{H_2O}}} \quad (16)$$

For $O_2$ reduction, the Tafel equation in terms of $O_2$ surface concentration $c_{7s}$ is:

$$i_{O_2s} = -i^0_{O_2ref}\frac{c_{7s}}{c_{7ref}} 10^{\frac{-(E-E^{Eqref}_{O_2})}{b_{O_2}}} \quad (17)$$

When the reference condition is taken at the holiday mouth so that the electrode potential is expressed as $E_m$ and the electrostatic potential of solution is set as $\varphi_m$=0, the electrode potential anywhere inside the crevice E can be expressed by the electrostatic potential of the solution $\varphi$:

$$\varphi = E_m - E \quad (18)$$

Thus, the Tafel equations for the anodic and cathodic half cell reactions may be written as:

$$i_{Fe} = i_{Fem} 10^{\frac{-\varphi}{b_{Fe}}} \quad (19)$$

where subscript "m" is referred to as the quantity at the holiday mouth.

For reductions of hydrogen ion and water, their Tafel equations can be expressed respectively as:

$$i_H = i_{Hm}\frac{c_4}{c_{4m}} 10^{\frac{\varphi}{b_H}} \quad (20)$$

and

$$i_{H_2O} = i_{H_2Om} 10^{\frac{\varphi}{b_{H_2O}}} \quad (21)$$


Copyright © 2010 by ASME

For $O_2$ reduction, the Tafel equation of Equation (17) can be written as:

$$i_{O_2 s} = i_{O_2 sm} \frac{c_{7s}}{c_{7sm}} 10^{\frac{\varphi}{b_{O_2}}} \tag{22}$$

where,

$$i_{O_2 sm} = -i^0_{O_2 ref} \frac{c_{sm}}{c_{ref}} 10^{\frac{-(E_m - E^{Eqref}_{O_2})}{b_{O_2}}} \tag{23}$$

*Model Initial and Boundary Conditions*

The initial and boundary conditions for solving the above equations are given in Table 1, where only concentrations of the primary species are given with the realization that the concentrations of the secondary species can be calculated from the concentrations of the primary species with use of the formula given in Appendix A.

As discussed earlier, the concentrations of $Na^+$ and $Cl^-$ at the mouth are assumed to be greater than at time zero in the disbonded region (initial condition). The solution is saturated by $Fe(OH)_2$ with the pH of approximately 9.2 both at the mouth and at time zero in the disbonded region. This pH is greater than in the bulk soil due to CP or oxygen and water reductions occurring at the steel surface. The bulk soil is assumed to be neutral with a pH 7 and has the same $Na^+$ and $Cl^-$ concentrations as at the holiday. When the $Na^+$ and $Cl^-$ concentrations are given, the electroneutrality ($\sum_j z_j c_j = 0$) and the saturation of the solution by $Fe(OH)_2$ can allow all other species to be determined.

The boundary condition at the crevice mouth is that the concentrations of all solution species are constant, invariant with time. The applied potential there can be either determined in the case of no CP or it is given as a fixed value when CP is present. The boundary conditions at the crevice tip are zero flux for each species and zero current flow (or zero gradient of the electrode potential), due to a coating that is impermeable to ionic and molecular species.

*Methods of Solving the Model Equations*

Equations (3-7) and (11) can be solved simultaneously to obtain all concentrations of the independent species ($c_1$, $c_2$, $c_4$ and $c_7$) and the potential ($\phi$ or E), where Equation (6) can be replaced by Equation (12).

A commercial finite element method code: Comsol 3.5 was used to solve the above equations. This code allows for flexible meshing of the model geometry and flexible setting of time steps. Since the gradients of concentrations and that of the potential are very large near the crevice mouth, the mesh there is arranged very dense. The time steps near time zero are designed to be very small.

Once the concentrations of the primary species are computed, by substitution of them into the equilibrium equations given in Appendix A, the concentrations of the secondary species can be determined.

Only the shaded scenarios shown in Table 3 are presented here, although all scenarios in the table have been investigated. The focus is the effect on crevice chemistry and corrosion potential and rate by the change of crevice gap vs. distance (x). The first scenario in the table has been investigated extensively earlier[13], while the condition with different initial concentrations between the holiday and in the disbonded region was not. A comparison of the results between these two scenarios is presented first.

## COMPUTATIONAL RESULTS

*Constant Crevice Gap*

Mouth Potential Fixed at -0.8071 $V_{CSE}$ with Negligible CP: Extensive study was performed previously with the case No. 1 in Table 3 when the mouth boundary concentrations and the initial concentrations are the same.[13] These concentrations are shown in the last row of Table 1. The tail boundary condition is shown one row above.

As already discussed earlier, when the holiday is created after the coating is disbonded, it is possible that the $Na^+$ and $Cl^-$ concentrations in the crevice may initially be smaller than those at the mouth. It would be useful to understand how this difference in concentrations of $Na^+$ and $Cl^-$ would affect the evolution of the crevice chemistry and corrosion potential and rate. In this study, the $Na^+$ and $Cl^-$ concentrations are assumed to be uniform initially in the entire crevice and equal in value. Their initial concentrations are one tenth of their concentrations at the mouth. The initial condition is shown in the 2nd row of Table 1. The mouth boundary condition is shown in the 3rd row for the presence of CP with a fixed mouth potential or the 4th row when CP is absent. The crevice tail boundary condition is shown in the row next to the last: zero flux for each species and zero current flow.

It is noted that, as shown by Table 1, the pH (or $c_4$) at the mouth used in this work (3rd row) is only slightly different from the previous work[13] (last row) and thus, the results of the previous work can be reproduced approximately by the current model when the $Na^+$ and $Cl^-$ initial concentrations are set to be the same as their concentrations at the mouth. Throughout this section, the reproduced results are mentioned as results of "previous work".

Figure 2a shows the $Na^+$ and $Cl^-$ concentrations in the crevice obtained in the previous work. The fixed mouth potential of -0.8071 $V_{CSE}$ was used at the mouth to represent a condition with initially no CP or negligible polarization. The mouth boundary condition used here is the 3rd row in Table 1.

Due to the presence of oxygen at the mouth, the steel potential at the mouth is more positive than inside the crevice. Inside the crevice near the mouth oxygen is depleted by corrosion. This oxygen reduction near the mouth functions as an imposed anodic polarization at the mouth, which draws out


Copyright © 2010 by ASME

of $Na^+$ from and pumps $Cl^-$ into the crevice. Because the mouth and the initial chemistries are the same, this seemingly anodic polarization has led to a decreasing $Na^+$ concentration, or increasing $Cl^-$ concentration, inside the crevice as time increases (Figure 2a).

When the $Na^+$ and $Cl^-$ concentrations at the mouth are 10 times of those initially in the crevice, the change of their concentrations vs. x is shown in Figures 2b and c to be sharp at the mouth at time zero. This sharp change of concentrations leads to a large diffusion rate from the mouth into the crevice for both $Na^+$ and $Cl^-$.

Unlike in Figure 2a where the $Na^+$ concentration in the crevice decreases over time, Figure 2b shows that the $Na^+$ concentration in the crevice increases over time, powered by its diffusion. Although $Na^+$ migration controlled by the potential gradient imposed by the (seemingly anodic) polarization depresses $Na^+$ concentration in the crevice, this effect is less significant than diffusion near the mouth. This effect of $Na^+$ migration can be seen on the curve of $10^4$ s, where the $Na^+$ concentration deep in the crevice drops below zero (initial condition). Although the $Na^+$ migration can occur immediately after time zero, the slow $Na^+$ diffusion cannot. The $Na^+$ diffusion would not occur deep in the crevice until after quite some time when a concentration gradient is created by the $Na^+$ migration and corrosion reactions.

Due to the different initial conditions between Figures 2a and b, the $Na^+$ concentration in the crevice varies differently. In Figure 1a, the $Na^+$ concentration tends to decrease over time controlled by migration, while in Figure 1b, $Na^+$ concentration changes in an opposite direction due to its diffusion from the mouth. Nevertheless, overall the $Na^+$ concentration decreases from the mouth into the crevice in both conditions. At $10^7$ s, when the corrosion process approximately reaches steady state, the two curves in both conditions become overlapped as shown in Figure 1b, verifying that the steady state condition of the corrosion process is not affected by the different initial conditions.

Unlike $Na^+$, Figure 2c shows that by carrying negative charge, the diffusion and migration of $Cl^-$ both tend to increase its concentration over time in the crevice. Although diffusion is more dominant initially near the mouth, migration is more inside the crevice. With time when the in crevice $Cl^-$ concentration becomes close to or greater than that at the mouth, the diffusion to increase $Cl^-$ concentration diminishes and the $Cl^-$ transport is mainly powered by migration.

With the disadvantage initially with a lower concentration than in the previous work, the $Cl^-$ concentration keeps being smaller than in the previous work as shown by the pair curves at $10^5$ s and $10^6$ s. This situation continues until steady state is reached at $10^7$ s and the two pair curves are overlapped. Due to the presence of oxygen at the mouth, the $Cl^-$ concentration in the crevice is greater than at the mouth.

Even though the initial and mouth pHs are the same initially for both this model and the previous model as shown in Figure 3, due to above variation of $Na^+$ and $Cl^-$ concentrations, which simultaneously affect or are affected by the concentrations of other secondary species including $Fe^{2+}$, the variations of pHs are different as seen in Figure 3. Nevertheless, this difference eventually diminishes at steady state at $10^7$ s, shown by the overlapped curve.

Figure 4a shows the corrosion potential and current density in the crevice at different times obtained in the previous work. Overall, their variations at the steady state condition are not significantly different from those at their initial condition. With oxygen being the main driving force for the corrosion process, the corrosion current density decreases from the holiday into the crevice and the corrosion potential correspondingly shifts in the more negative direction.

The difference between this model and the previous model is mainly shown at time zero in Figure 4b for potential and in Figure 4c for corrosion current density. This difference results from the sharp change of the solution chemistry at the mouth immediately after time zero. This requires a significant change of crevice potential and correspondingly corrosion current density to compensate for the sudden change of chemistry. With time, this difference is shown to decrease quickly as the chemistry becomes smoother in the crevice. By the time about $10^5$ s, this difference nearly vanishes on the scales of the charts.

By fixing the mouth potential at -0.8071 $V_{CSE}$ as modeled above, it is assumed that the variation of the mouth potential with time due to variation of chemistry can be neglected. This assumption may be verified next.

<u>Time-Varying Mouth Potential at No CP:</u> When there is no CP, the mouth potential can vary with time due to change of the chemistry inside the crevice. The only difference between modeling this no-CP condition and modeling the condition with a fixed mouth potential is the mouth boundary condition for potential. All other mouth boundary conditions, the initial condition and the crevice tail boundary condition are still the same. The no CP mouth boundary condition corresponds to the 4th row of Table 1 (current passing the mouth is zero) while the fixed potential at the mouth corresponds to the boundary condition shown in the row above. A comparison of the model results obtained in these two conditions is untaken. The variation of the mouth potential with time at the condition of no CP is presented first.

Figure 5 shows the variation of the crevice mouth potential vs. time when there is no CP at the mouth. The mouth potential varies within the small range of -0.7929 ~ -0.8087 $V_{CSE}$. In this semi-log diagram, although some variation is shown near time zero, the seemingly more significant potential drop occurs after approximately 5 s. The total potential drop within $10^7$ s is less than 16 mV, caused by the change of solution chemistry in the crevice. The mouth potential of -0.8071 $V_{CSE}$ used in the previous section is shown to fall within this narrow window of mouth potential.

Figure 6 shows a comparison of the $Na^+$ concentration and pH obtained with no CP and with a fixed mouth potential of -


Copyright © 2010 by ASME

0.8071 $V_{CSE}$. For the different times given in the charts, nearly no difference can be seen with the $Na^+$ concentration or a small difference only at $10^2$ s with pH.

Although an obvious difference is shown at time zero for potential in Figure 7a and for corrosion current density in Figure 7b, the difference afterwards decreases and becomes invisible at $10^5$ s and forward.

It is clear from the above analysis that it appears valid to use a fixed mouth potential of -0.8071 V to approximate the no CP condition for the case investigated.

Fixed Mouth Potential at -0.9 $V_{CSE}$: The crevice chemistry and corrosion potential and rate at the mouth potential of -0.9 $V_{CSE}$ was investigated in detail elsewhere,[13] where the mouth chemistry is the same as the initial in the crevice. At this potential, the crevice mouth is cathodically polarized.

Figure 8a shows the $Na^+$ and $Cl^-$ concentrations obtained in previous work at the mouth potential of -0.9 $V_{CSE}$. The $Na^+$ and $Cl^-$ concentrations are shown to change with time in opposite direction; $Na^+$ concentration in the crevice increases while that of $Cl^-$ decreases.

Figure 8b shows the $Na^+$ concentration obtained in this work with the mouth chemistry different from it initially in the crevice. The synergistic diffusion and migration of $Na^+$ into the crevice leads to an increase of $Na^+$ concentration over time in the crevice. Although the $Na^+$ concentration obtained in this model is overall smaller than that obtained from the previous model due to a smaller initial concentration with this model, their difference in $Na^+$ concentration decreases over time and nearly disappears at $10^7$ s. This variation of $Na^+$ concentration here is rather similar to the variation of $Cl^-$ concentration shown in Figure 2c with the mouth potential of -0.8071 $V_{CSE}$, due to the fact that these two ions have opposite sign of charge and the correspondingly external polarizations (or external current flow directions) between the two cases are opposite. These two factors cancel each other in the migration term of the flux equation.

Figure 9 shows a comparison of crevice pHs obtained from this model and the previous model. Both crevice pHs increase over time. For the times shown in the figure, the largest difference between these two pHs is shown at $10^4$ s. At $10^7$ s, steady state is reached and the two curves are overlapped.

Figure 10 shows a comparison of the crevice potential and current density at different times obtained from this model and previous model. The significant difference at time zero results from the sudden change of chemistry at the mouth after time zero, similar to what was explained for Figure 4 earlier. At $10^7$ s, the two curves are merged irrespective of their different initial conditions.

*Crevice Gap Varying with Distance (x)*

In the field, a well-defined rectangle crevice is rarely seen even though such geometry has been most frequently used in crevice corrosion studies. The real crevice gap always varies with distance in the longitudinal direction, and each crevice has a unique geometry. In this study, a crevice with its gap varying in the longitudinal direction is used. To understand the effect by crevice geometries, a sharp change of the gap with distance (Figure 1b) and a smoother change of the gap (Figure 1c) are used here. In this work, Figure 1b is chosen to be the focus of the modeling because its sharp gap variation would have a greatest effect on crevice corrosion.

In the sections below, the effect of the gap variation on the crevice chemistry, potential and corrosion current density is presented. The effect with no CP is presented first, followed by the effect with CP imposed at the crevice mouth.

Mouth Potential at -0.8071 $V_{CSE}$ (Figures 1a and 1b): Without CP at the crevice mouth, Figure 11a shows the $Na^+$ concentrations obtained near the crevice mouth for the two crevice geometries shown in Figures 1a and 1b. The concentrations obtained from these two crevices are shown to be the same until after $10^2$ s when the change of gap is reached at $\frac{x}{\delta_{s0}}$=5. At $10^4$ s and $10^7$ s, a steeper decrease of $Na^+$ concentration is seen in the region of narrowed gap in $\frac{x}{\delta_{s0}}$=5-6. Compared to the $Na^+$ concentration obtained for the crevice of constant gap (Figure 1a), the $Na^+$ concentration in the crevice of variable gap is greater around $\frac{x}{\delta_{s0}}$=5 but is smaller around $\frac{x}{\delta_{s0}}$=6. This effect may be explained by treating $Na^+$ transport in the crevice as flow or the $Na^+$ flux as velocity. The flux of $Na^+$ becomes increasingly greater as moving from the crevice mouth to the left edge of the gap-narrowed region, and thus, $Na^+$ tends to accumulate around the left edge of gap-narrowed region. When the gap suddenly expands at $\frac{x}{\delta_{s0}}$=6, the $Na^+$ flux decreases and $Na^+$ tends to dissipate out from the gap-narrowed region to the region with a wider gap, leading to a decrease of $Na^+$ concentration relative to that in the crevice of constant gap.

The above variation of $Na^+$ concentration across the first gap-narrowed region is also similarly shown in Figure 11b across the second gap-narrowed region in $\frac{x}{\delta_{s0}}$=15-100. In Figure 11b, the y axis was scaled up because the difference in $Na^+$ concentration deep in the crevice is smaller and would otherwise not be seen clearly if plotted together with Figure 11a.

The change of $Na^+$ concentration in the range of $\frac{x}{\delta_{s0}}$=5-6 is shown to be greater than in the range of $\frac{x}{\delta_{s0}}$=15-100 because the $Na^+$ concentration gradient is greater near the mouth and the impact on this gradient by the sharp change of gap is also greater. Even with a steeper change of $Na^+$ concentration due to the sharp change of gap (relative to a constant crevice gap), the $Na^+$ concentration obtained from the two different geometries (Figure 1a and b) are overall not significantly different. Within these two regions of narrowed


Copyright © 2010 by ASME

gap ($\frac{x}{\delta_{s0}}$=5-6 and 15-100), the change of $Na^+$ concentration at $10^7$ s is smoother or less steep than at $10^4$ s because more time is available for the transport of $Na^+$ from the mouth.

Overall, Figure 11a and b suggests that the effect of variable gap for the case studied here is not significant. It is expected that this effect would be greater if the gap-narrowed region near the mouth is expanded.

Figures 12a and b shows a comparison of the crevice pHs at different times for the two crevice geometries shown in Figures 1a and b. Although the sharp change of the crevice gap has resulted in a different pH relative to that obtained with a constant crevice gap, the overall difference between the pHs obtained from these two crevice geometries is shown to be not significant. The difference in the pHs occurs mainly within the two regions of narrowed gap in $\frac{x}{\delta_{s0}}$=5-6 and 15-100.

The results from Figures 11 and 12 suggest that the difference in the crevice geometries of Figures 1a and b does not result in a significant effect on the crevice chemistry. Thus, it is expected that this effect on the crevice potential and corrosion rate would also not be significant.

Figure 13 shows a comparison of the crevice potentials obtained with the two crevice geometries shown in Figure 1a and b. Although the sharp change of gap results in a clear change of the potential near the mouth (relative to the potential in the crevice of constant gap), deep in the crevice at $\frac{x}{\delta_{s0}}$=100 the effect by the sharp change of the gap is seen to be insignificant. Since the above effect is local, only at or near the regions of narrowed gap the overall difference in potential is seen but small.

The variation of crevice corrosion current density is similar to that of the crevice potential and shown in Figure 14a near the mouth and 14b deeper inside the crevice. Even though the difference between corrosion current densities obtained from these two crevice geometries is shown to be more significant at $10^7$ s than at time zero, the difference is in general small.

Mouth Potential at -0.9 $V_{CSE}$ (Figures 1a-c): Figure 15 shows $Na^+$ concentrations obtained by using all three crevice geometries shown in Figure 1. Figure 15a shows the results in the entire crevice and Figure 15b shows only the results near the mouth. Overall, the difference in $Na^+$ concentration in the entire crevice for the three different crevice geometries is insignificant. At $10^8$ s, the $Na^+$ concentration in the crevice with constant gap is shown to be smaller inside the crevice (relative to the two crevices of variable gap), while it is slightly greater near the holiday. In the crevices with variable gap, it requires $10^8$ s for the crevice corrosion to reach steady state. This time is longer than for the crevice of constant gap, which requires only $10^7$ s for its corrosion to reach steady state.

Figure 15b shows that across the gap-narrowed region ($\frac{x}{\delta_{s0}}$=5~6), the $Na^+$ concentration has a steeper variation with distance (relative to the crevice of constant gap). The sharp change of $Na^+$ concentration occurs at the points of gap change. The more gradual gap variation in $\frac{x}{\delta_{s0}}$=15-100 associated with the crevice shown in Figure 1c shows a more gradual variation of $Na^+$ concentration relative to variation in the crevice shown in Figure 1b with a sharp gap change.

For the first region of narrowed gap in $\frac{x}{\delta_{s0}}$=5~6, Figure 15b shows that at $10^3$ s, $Na^+$ transport just passes through this region and has not yet reached the 2nd gap-narrowed region in $\frac{x}{\delta_{s0}}$=15~100. With the same geometry of the two crevices shown in Figure 1b and c, the $Na^+$ concentrations in these two crevices are seen overlapped. The $Na^+$ concentration in these crevices around the left edge of the narrowed region is shown to be higher than that in the crevice of constant gap. This difference in $Na^+$ concentration among the crevices is the result of significant increase of flux caused by the sudden reduction of the crevice gap at $\frac{x}{\delta_{s0}}$=5. This increased flux leads to accumulation of $Na^+$ around the left edge of the narrowed gap. On the contrary, at the sudden expansion of the gap at $\frac{x}{\delta_{s0}}$=6, a reverse effect dominates. $Na^+$ more easily transports out from the gap-narrowed region and the $Na^+$ concentration after the right edge of the gap-narrowed region becomes smaller (relative to the crevice of constant gap).

Similar increase of $Na^+$ concentration occurs at the left edge of the second gap-narrowed region ($\frac{x}{\delta_{s0}}$=15) at $10^4$ s. By contrast, with a gradual decrease of gap for the crevice in Figure 1c, the $Na^+$ concentration does not become greater than in the crevice of constant gap until after $\frac{x}{\delta_{s0}}$=20. This smaller concentration is the result of the residual effect from the reduced $Na^+$ concentration around the right edge of the first gap-narrowed region. This $Na^+$ concentration in the crevice with gradual gap reduction eventually exceeds the concentration in the crevice of constant gap because of the gradually increasing $Na^+$ flux as the gap continues to narrow down.

At $10^5$ s, the $Na^+$ transport still does not pass though the right edge of the 2nd gap-narrowed region as shown in Figure 15a, where at $\frac{x}{\delta_{s0}}$=100, the $Na^+$ concentration is still approximately that in the initial condition. Due to accumulation of $Na^+$ in the crevice of variable gap before the right edge of the second gap-narrowed region ($Na^+$ transport limited by the narrowed gap), the $Na^+$ concentration in crevices of narrowed gap is overall greater than in the crevice of constant gap.

Once the $Na^+$ transport passes through the right edge of the second gap-narrowed region, the $Na^+$ concentration gradient in the crevice becomes smoother over time. At time $10^6$ s, limited by the narrowed gap $Na^+$ still accumulates in the crevices of variable gap near the mouth and thus, the $Na^+$ concentration in these crevices is greater than in the crevice of


Copyright © 2010 by ASME

constant gap. By the same token, with less limitation of $Na^+$ transport into the crevice of constant gap, the $Na^+$ concentration deep in this crevice is greater than in the crevices of variable gap.

The above analysis suggests that with CP, the narrowing of gap appears to push $Na^+$ into the region of narrowed gap while conversely the gap expansion appears to draw out $Na^+$ concentration into region of larger gap. This effect is stronger near the mouth because of a greater flux.

The crevice with a narrowed gap appears to behave like a longer crevice of constant gap. Thus, a longer time is needed for the crevices with narrowed gap to reach steady state than the crevice of constant gap. For the crevice of constant gap, $10^7$ s is needed while for the crevices of variable gap, it is shown that $10^8$ s is required. At $10^8$ s, Figure 15a shows that the $Na^+$ concentration in the crevice of variable gap eventually becomes greater than in the crevice of constant gap. The more narrowed crevice of Figure 1b also has a higher $Na^+$ concentration than the crevice of Figure 1c.

Figure 16 shows a comparison of the pHs in the above three crevices at different times. Similar to the variation of $Na^+$ concentration, sharp change of pH occurs at the edges of gap change. Although this cannot be clearly seen in the first gap-narrowed region in $\frac{x}{\delta_{s0}}$=5-6 because the pH change there is steep (even in the crevice of constant gap). The steeper change of pH in the crevice of variable gap (relative to the crevice of constant gap) is more clearly shown in the second gap-narrowed region associated with the crevice of Figure 1b at $\frac{x}{\delta_{s0}}$=15 and 100 where the gap suddenly narrows. With a more gradual variation of gap in Figure 1c, at $10^6$ s the pH variation is shown to be smoother relative to the crevice with a sharp gap change shown in Figure 1b. Overall, the effect of variable gap on the crevice pH is not significant for the conditions studied.

Figure 17 shows (a) crevice potentials and (b) corrosion current densities at different times for the three crevices. In general, the effect of variable gap on these two parameters is not significant.

## CONCLUSIONS

A comprehensive mathematical model is developed that allows for predicting chemistry and corrosion in a crevice which may have the boundary chemistry different from at the initial condition and the crevice gap vary with distance.

Due to the specific crevice geometry used in this modeling - a small of area externally polarized (the crevice mouth), the overall change of solution chemistry and corrosion potential and rate in the crevice of varying gap is not significant relative to the change in the crevice of constant gap.

In a crevice of variable gap, the gap change appears to provide a pumping effect of ions relative to a crevice of constant gap. With CP, a sharp decrease of gap appears to push in $Na^+$ into the gap-narrowed region while a sharp expansion of gap appears to draws out of $Na^+$.

## PRACTICAL IMPLICATIONS OF THE RESULTS

Understanding the level of CP, chemistry and corrosion rate in a coating-disbonded region is technically challenging. A modeling tool is developed in this work based on fundamental principles. This model can allow for simulating the evolution over time of the chemistry, corrosion potential and rate in a coating-disbonded region.

The model results show that when a holiday is protected with CP, the pH in the coating-disbonded region increases over time and the corrosion rate decreases. Given a sufficient time, this pH increase can go farther into the disbonded region and even becomes higher than at the holiday if the CP is continuously maintained at the holiday.

For a field disbonded region, the actual gap always varies with distance from the holiday. The effect of the varying gap on the corrosion conditions in the coating-disbonded region was investigated. With CP, at the location where the gap narrows the cation (e.g. $Na^+$) concentrations tend to be greater than if the gap is constant. By contrast, the anion (e.g. $Cl^-$) concentrations tend to be smaller. Conversely, at the location of gap expansion, the cation concentrations tend to be smaller or the anion concentrations tend to greater (relative to a disbonded region of constant gap). With a reduction of 25% reduction of gap for a small segment of the disbonded region, the effect of the gap change appears to be not significant.

The above results suggest that the field techniques developed earlier[39] for evaluating CP penetration limit and for estimating the distributions of corrosion potential and rate in a coating disbonded region (constant gap) can be applied to a disbonded region of variable gap. In using the field methods, the values of the variable gap need to be averaged approximately.

## ACKNOWLEDGMENTS

This work was sponsored by the US Department of Transportation, Pipeline and Hazardous Materials Safety Administration (Mr. James Merritt, Program Manager), under the contract: DTPH56-08-T-0003. It was co-funded by Pipeline Research Council International (Mr. Mark Piazza, Senior Program Manager) and CenterPoint Energy, New Orleans, LA. (Mr. Rickey Payne, Direct Assessment Manager).

## REFERENCES

1. H. Leidheiser, W. Wang, L. Igetoft, Progress in Organic Coatings 11 (1983) 19-40.
2. C.G. Munger, Corrosion Prevention by Protective Coatings (NACE, 1984) 47-61.
3. J.M. Leeds, Pipe Line & Gas Industries, March (1995) 21-26.
4. M. Meyer, X. Campaignolle, F. Coeuille, M.E.R. Shanahan, "Impact of Aging Processes on Anticorrosion properties of Thick Polymer Coatings for Steel Pipelines", in Proceedings of the Corrosion/2004 Research topical Symposium: Corrosion Modeling for Assessing the


Copyright © 2010 by ASME

Condition of Oil and Gas Pipelines, F. King and J. Beavers (eds.), Houston, TX: NACE/2004, 93-146.
5. F.M. Song, "Corrosion of Coated Pipelines with Cathodic Protection", Ph.D. thesis (2002), University of Toronto, Department of Chemical Engineering and Applied Chemistry.
6. F.M. Song, D.W. Kirk, D.E. Cormack, D. Wong, Materials Performance, 44 (4) (2005) 26-29.
7. F.M. Song, D.W. Kirk, D.E. Cormack, D. Wong, Materials Performance, 42(9) (2003) 24-26.
8. F.M. Song, D.W. Kirk, J.W. Graydon, D.E. Cormack, Corrosion 58(12) (2002) 1015-1024.
9. F.M. Song, D.W. Kirk, J.W. Graydon, D.E. Cormack, Corrosion 59(1) (2003) 42-49.
10. F.M. Song, D.A. Jones, D.W. Kirk, Corrosion, 60(2) (2005) 145-154.
11. F.M. Song, N. Sridhar, Corrosion 62(8) (2006) 676-686.
12. F.M. Song, N. Sridhar, Corrosion 62(10) (2006) 873-882.
13. F.M. Song, N. Sridhar, Corrosion Science 50(1) (2008) 70-83.
14. N. Sridhar, D.S. Dunn, M. Seth, 2001, Corrosion 57 (7), 598-613.
15. N. Sridhar, "Modeling the Conditions under Disbonded coating Crevices – A Review", in Proceedings of the Corrosion/2004 Research topical Symposium: Corrosion Modeling for Assessing the Condition of Oil and Gas Pipelines, F. King and J. Beavers (eds.), Houston, TX: NACE/2004, 53-92.
16. Orazem, M.E., D.P. Reimer, C. Qiu, K. Allahar, "Computer Simulations for Cathodic Protection of Pipelines", in Proceedings of the Corrosion/2004 Research topical Symposium: Corrosion Modeling for Assessing the Condition of Oil and Gas Pipelines, F. King and J. Beavers (eds.), Houston, TX: NACE/2004, 25-52.
17. R.R. Fessler, A.J. Markworth, R.N. Parkins, Corrosion 39 (1) (1983) 20-25.
18. T.R. Jack, G.V. Boven, M. Wilmott, R.L. Sutherby, R.G. Worthingham, MP (8) (1994) 17-21.
19. A. Turnbull, A.T. May, Materials Performance, 22 (1983) 34.
20. J.J. Perdomo, I. Song, Corrosion Science 42 (2000) 1389.
21. M.H. Peterson, T.J. Lennox, Jr., Corrosion 29 (1973) 406.
22. A.C. Toncre, N. Ahmad, Materials Performance 19(6) (1980) 39.
23. M.D. Orton, Materials Performance 24(6) (1985) 17.
24. F. Gan, Z.-W. Sun, G. Sabde, D.-T. Chin, Corrosion 50(10) (1994) 804.
25. R. Brousseau, S.Qian, Corrosion 50 (12) (1994) 907-911.
26. F. King, T. Jack, M. Kolar, and R. Worthingham, "A Permeable Coating Model for Predicting the Environment at the Pipe Surface under CP-Compatible Coatings", NACE/04, paper no. 04158.
27. F.M. Song, Corrosion Science 50 (2008) 3287-3295.
28. F.M. Song, D.W. Kirk, J.W. Graydon, D.E. Cormack, Corrosion 58(2) (2002) 145-155.
29. R. Parsons, Handbook of Electrochemical Constants (London: Butterworths Scientific Publications, 1959) 47 and 66.
30. D. Tromans, Corrosion 55 (1999) 942.
31. J. Newman and K.E. Thomas-Alyea, Electrochemical Systems, 3rd ed. (Englewood Cliffs, NJ: Prentice Hall, 1991).
32. J. Kvarekval, "A Kinetic Model for Calculating Concentration Profiles and Fluxes of CO2-Related Species across the Nernst Diffusion Layer", Corrosion/97, Paper no. 5 (Houston, TX: NACE 1997).
33. V. Jovancicevic, J. O'M. Bockris, J. Electrochem. Soc. 133 (1986) 1797.
34. S. Nesic, J. Postlethwaite, S. Olsen, Corrosion 52 (1996) 280.
35. J.O'M. Bockris, D. Drazic, A.R. Despic, Electrochimica Acta 4 (1961) 325.
36. J.G.N. Thomas, T.J. Nurse, R. Walker, Br. Corros. J. 5 (1970) 87.
37. C.M. Shepherd, S. Schuldiner, J. Electrochem. Soc. 115 (1968) 1124.
38. M. Stern, R.M. Roth, J. Electrochem. Soc. 104 (1957) 390.
39. F.M. Song, Corrosion 66 (3) (2010) 035005.


Copyright © 2010 by ASME

## APPENDIX A

## REVERSIBLE AND IRREVERSIBLE HOMOGENEOUS AND HETEROGENEOUS REACTIONS IN THE SYSTEM, CHEMICAL EQUILIBRIUM FORMULA AND KINETIC RATES IN THE CREVICE CORROSION SYSTEM IN THE PRESENCE OF DISSOLVED $O_2$

The reversible reactions in the crevice are listed below. The reactions in the parentheses are equivalent reactions but show more clearly the equilibrium relations among reactants and products. The concentrations of all the secondary species can be expressed by those of the primary species as shown.

$$H_2O - H^+ \leftrightarrow OH^-$$
$$(H_2O \leftrightarrow H^+ + OH^-)$$
$$c_4 c_5 = K_w \tag{A.1}$$

$$Fe(OH)_2 + 2H^+ \leftrightarrow Fe^{2+} + 2H_2O$$
$$(Fe(OH)_2 \leftrightarrow Fe^{2+} + 2OH^-)$$
$$c_3 c_5^2 = K_{SP} \tag{A.2}$$

$$Fe(OH)_2 + H^+ \leftrightarrow FeOH^+ + H_2O$$
$$(Fe^{2+} + H_2O \leftrightarrow FeOH^+ + H^+)$$
$$\frac{c_4 c_6}{c_3} = K_1 \tag{A.3}$$

When the concentrations of $Na^+$ and $Cl^-$ are same, the electroneutrality ($\sum_j z_j c_j = 0$) and the above equations allow each concentration to be determined analytically.

The equation of electroneutrality is:

$$2K_{sp} + (K_w + \frac{K_1 K_{sp}}{K_w})c_5 - c_5^3 = 0 \tag{A.4}$$

The solution of Equation (A.4) is:

$$c_5 = \frac{2^{\frac{1}{3}}(k_w + \frac{K_1 K_{sp}}{K_w})}{\lambda_2} + \frac{\lambda_2}{3 \cdot 2^{\frac{1}{3}}} \tag{A.5}$$

where $\lambda_1 = 6\sqrt{81k_{sp}^2 - 3(k_w + \frac{K_1 K_{sp}}{K_w})^3}$

and $\lambda_2 = (\lambda_1 + 54k_{sp})^{\frac{1}{3}}$.

For a more general case where the charges of $Na^+$ and $Cl^-$ may or may not balance out, the equation below may be used:

$$z_1 c_1 + z_2 c_2 + z_3 \frac{K_{sp}}{c_5^2} + z_4 \frac{K_w}{c_5} + z_5 c_5 + z_6 \frac{K_1 K_{sp}}{K_w c_5} = 0 \tag{A.6}$$

Alternatively, it is written as:

$$z_5 c_5^3 + p_1 c_5^2 + p_{10} c_5 + z_3 K_{sp} = 0 \tag{A.7}$$

where $p_{10} = (z_4 K_w + z_6 \frac{K_1 K_{sp}}{K_w}) / z_5$, and $p_{20} = z_3 K_{sp} / z_5$.

The solution of Equation (A.7) is:

$$c_5 = -\frac{p_1}{3} - \frac{2^{\frac{1}{3}} p_2}{3p_5} + \frac{p_5}{2^{\frac{1}{3}} 3} = \frac{p_5^2 - 2^{\frac{1}{3}} p_1 p_5 - 2^{\frac{2}{3}} p_2}{2^{\frac{1}{3}} 3 p_5} \tag{A.8}$$

where,

$$p_5 = (p_3 + p_4)^{\frac{1}{3}} \tag{A.9a}$$
$$p_4 = \sqrt{27(4p_{10}^3 - 2p_{20}p_3 - (p_{10}p_1)^2 - 27p_{20}^2)}, \tag{A.9b}$$
$$p_3 = -2p_1^3 + 9p_{10}p_1 - 27p_{20}, \tag{A.9c}$$
$$p_2 = -p_1^2 + 3p_{10}, \tag{A.9d}$$
$$p_1 = (z_1 c_1 + z_2 c_2) / z_5. \tag{A.9e}$$

With Equation (A.5) or (A.8), the concentrations of other species may be calculated from:

$$c_4 = \frac{k_w}{c_5},\ c_3 = \frac{K_{sp}}{c_5^2},\ c_6 = \frac{K_1 K_{sp}}{K_w c_5} \tag{A.10}$$

The electrochemical reactions are:

$$Fe \rightarrow Fe^{2+} + 2e^- \qquad r_{Fe}^e \tag{A.11}$$

$$H^+ + e^- \rightarrow 0.5H_2 \qquad r_H^e \tag{A.12}$$

$$H^+ + e^- \rightarrow 0.5H_2 \qquad r_{H_2O}^e \tag{A.13}$$
$$(H_2O + e^- \rightarrow 0.5H_2 + OH^-)$$

$$4H^+ + O_2 + 4e^- \rightarrow 2H_2O \qquad r_{O_2}^e \tag{A.14}$$


Copyright © 2010 by ASME

## APPENDIX B

## SIMPLIFICATION OF 2D $O_2$ TRANSPORT BY USING A PARABOLIC RELATION

A parabolic relation may be used to express the oxygen concentration c vs. y across the gap shown in Figure 1a, b or c:

$$c = \alpha_1 y^2 + \beta_1 y + c_s \tag{B.1}$$

For a permeable coating, the boundary condition at the coating inner surface may be approximated by:

$$\left.\frac{\partial c}{\partial y}\right|_{y=\delta_s} = \frac{D_{O_2c}(c^0 - c_c)}{D_{O_2}\delta_c} = \frac{m(c^0 - c_c)}{\delta_s}, \tag{B.2}$$

where $m = \frac{\delta_s D_{O_2c}}{D_{O_2}\delta_c}$, $\delta_c$ is the coating thickness, $D_{O_2}$ and $D_{O_2c}$ are $O_2$ diffusivity in solution and coating respectively, and $c^0$ and $c_c$ are $O_2$ concentrations in solution located at the outer and inner surfaces of the coating respectively.

When the boundary condition at the steel surface:

$$-D_{O_2}\left.\frac{\partial c}{\partial y}\right|_{y=0} = r_{O_2} \quad (r_{O_2} \le 0). \tag{B.3}$$

is used, since the first derivative of Equation (B.1) over y is:

$$\frac{\partial c}{\partial y} = 2\alpha_1 y + \beta_1 \tag{B.4}$$

the following equations are obtained:

$$\beta_1 = -\frac{r_{O_2}}{D_{O_2}} \tag{B.5a}$$

and

$$\alpha_1 = \frac{m(c^0 - c_c)}{2\delta_s^2} - \frac{\beta_1}{2\delta_s} \tag{B.5b}$$

Since $c_c = \alpha_1\delta_s^2 + \beta_1\delta_s + c_s$ at the coating inner surface, by substitution of (B.5a) and (B.5b) and reorganization it is obtained that:

$$c_c = \frac{mc^0 + \beta_1\delta_s + 2c_s}{m+2} \tag{B.6}$$

Substitute Equations (22-23) into Equation (B.5a) to yield:

$$\beta_1 = \frac{\pi}{\delta_s} c_s, \tag{B.7}$$

where,

$$\pi = -\frac{\delta_s i_{O_2sm} 10^{\frac{\varphi}{b_{O_2}}}}{n_{O_2} F D_{O_2} c_{sm}} = -\frac{\delta_s^2}{\lambda} 10^{\frac{\varphi}{b_{O_2}}} \tag{B.7a}$$

if it is ordered that $\lambda = -\frac{\delta_s n_{O_2} F D_{O_2} c_{ref}}{i^0_{O_2ref} 10^{\frac{-(E_m - E_{O_2}^{Eqref})}{b_{O_2}}}}$.

Substitute Equation (B.7) into (B.6) to yield:

$$c_c = \frac{mc^0 + (2+\pi)c_s}{m+2} \tag{B.8}$$

Substituting (B.7-B.8) into (B.5b) yields:

$$\alpha_1 = \frac{mc^0 - (m+\pi+m\pi)c_s}{\delta_s^2(m+2)} \tag{B.9}$$

By averaging $O_2$ concentration in (B.1) and by use of Equations (B.7) and (B.9) the following equation is obtained:

$$\bar{c} = \frac{a^2\alpha_1}{3} + \frac{a\beta_1}{2} + c_s = \frac{mc^0}{3(m+2)} + \frac{4m+12+\pi m+4\pi}{6(m+2)} c_s,$$

or,

$$c_s = \frac{6(m+2)\bar{c} - 2mc^0}{4m+12+\pi m+4\pi} \tag{B.10}$$

Substitute (B.10) into (B.8) and (B.5a) to yield respectively,

$$c_c = \frac{6(\pi+2)\bar{c} + m(\pi+4)c^0}{4m+12+\pi m+4\pi} \tag{B.11}$$

and

$$r_{O_2} = -D_{O_2}\frac{\pi}{\delta_s} c_s = -\frac{D_{O_2}\pi[6(m+2)\bar{c} - 2mc^0]}{\delta_s(4m+12+\pi m+4\pi)} \tag{B.12}$$

The overall mass transport equation of oxygen can now be expressed by:

$$\begin{aligned} &\frac{\partial(\bar{c}\delta_s)}{\partial t} - \frac{\partial}{\partial x}\left(D_{O_2}\delta_s\frac{\partial\bar{c}}{\partial x}\right) \\ &= D_{O_2}\left(\frac{m(c^0 - c_c)}{\delta_s} + \frac{r_{O_2}}{D_{O_2}}\right) \\ &= \frac{2D_{O_2}[3m(\pi+2)c^0 - 6(m+\pi+m\pi)\bar{c}]}{\delta_s(4m+12+\pi m+4\pi)} \end{aligned} \tag{B.13}$$


Copyright © 2010 by ASME

At the mouth, φ=0 and Equation (B.7a) becomes

$$\pi_m = -\frac{\delta_s i_{O_2 sm}}{n_{O_2} F D_{O_2} c_{sm}} = -\frac{\delta_s^2}{\lambda} \qquad \text{(B.14)}$$

where $\pi_m$ is $\pi$ at the crevice mouth.

With $c_c=c^0$ at the mouth, Equation (B.8) at the mouth becomes

$$c^0 = \frac{mc^0 + (2+\pi_m)c_{sm}}{m+2}, \qquad \text{(B.15)}$$

or

$$c_{sm} = \frac{2c^0}{2+\pi_m} = \frac{2\lambda c^0}{2\lambda - \delta_s^2} \qquad \text{(B.16)}$$

If applied at the mouth, with $c_c=c^0$ Equation (B.11) becomes

$$\bar{c}_m = \frac{2(3\lambda - \delta_s^2)c^0}{3(2\lambda - \delta_s^2)} \qquad \text{(B.17)}$$

or

$$\lambda = \frac{\delta_s^2}{6}\frac{2c^0 - 3\bar{c}_m}{c^0 - \bar{c}_m} \qquad \text{(B.17a)}$$

Substitute Equation (B.17a) into Equations (B.16) and (B.12) to yield respectively

$$c_{sm} = \frac{3\lambda \bar{c}_m}{(3\lambda - \delta_s^2)} \qquad \text{(B.18)}$$

and

$$r_{O_2 m} = -D_{O_2}\frac{\pi_m}{\delta_s} c_{sm} = \frac{3D_{O_2}\delta_s \bar{c}_m}{3\lambda - \delta_s^2} \qquad \text{(B.19)}$$

When approximation is applied for $r_{O_2 m}$ by assuming oxygen diffusion controls so that $\lambda >> \delta_s^2$, Equations (B.17) and (B.19) become respectively,

$$\bar{c}_m = \frac{2c^0}{3} \qquad \text{(B.20a)}$$

and

$$r_{O_2 m} \cong -\frac{3D_{O_2}\bar{c}_m}{\delta_s} \cong -\frac{2D_{O_2}c^0}{\delta_s} \qquad \text{(B.20b)}$$


Copyright © 2010 by ASME

**Table 1: Initial and Boundary Conditions in This and a Previous Work**

| *Condition* | $c_1$ *(mol/m³)* | $c_2$ *(mol/m³)* | $c_4$ *(mol/m³)* | $c_7^0$ *(mol/m³)* | $\phi$ *or* $i_{tot}$ *(V)* *(A/m²)* |
|---|---|---|---|---|---|
| Initial | 0.3128 | 0.3128 | $6.014\times10^{-7}$ | 0* | |
| Mouth with CP | 3.128 | 3.128 | $6.014\times10^{-7}$ | 0.2601 | 0 |
| Mouth no CP | 3.128 | 3.128 | $6.014\times10^{-7}$ | 0.2601 | $i_{totx}=0$ |
| Bulk soil | 3.128 | 3.128 | $10^{-4}$ | 0.2601 | 0 |
| *Condition* | $N_{1x}$ (mol/m²·s) | $N_{2x}$ (mol/m²·s) | $N_{2x}$ (mol/m²·s) | $N_{2x}$ (mol/m²·s) | $i_{totx}$ (A/m²) |
| Crevice tail | 0 | 0 | 0 | 0 | 0 |
| *Previous work[13]* | $c_1$ *(mol/m³)* | $c_2$ *(mol/m³)* | $c_4$ *(mol/m³)* | $c_7^0$ *(mol/m³)* | $\phi$ *(V)* |
| Initial and mouth | 0.3128 | 0.3128 | $6.31\times10^{-7}$ | 0.2601 | 0 |

**: This value may be determined from $O_2$ diffusion via coating at steady state (prior to holiday formation).*

**Table 2: Constants and Values of Parameters Used for the Modeling**

| *Symbol* | *Value* | *Units* | *Explanation* | *Ref* |
|---|---|---|---|---|
| **Physical parameters** | | | | |
| $T$ | 298.15 | K | System temperature | |
| **Constants** | | | | |
| $F$ | 96485 | C/mol | Faraday's constant | 29 |
| $R$ | 8.3143 | J/mol·K | Gas constant | 29 |
| **Thermodynamic constants** | | | | |
| $K_w$ | $10^{-8}$ | $(mol/m^3)^2$ | Water ionic product | 29 |
| $K_1$ | $3.16\times10^{-7}$ | $mol/m^3$ | Equilibrium constant for $Fe^{2+}+H_2O\rightarrow Fe(OH)^+ + H^+$ | # |
| Ksp | $1.82\times10^{-6}$ | $(mol/m^3)^3$ | Solubility product of $Fe(OH)_2$ | 29 |
| $H_{O_2}$ | 0.8074 | $atm\cdot m^3/mol$ | Henry's law constant for $O_2$ | 30 |
| **Diffusion coefficients** | | | | |
| $D_{Na^+}$ | $1.334\times10^{-9}$ | $m^2/s$ | $Na^+$ | 31 |
| $D_{Cl^-}$ | $2.032\times10^{-9}$ | $m^2/s$ | $Cl^-$ | 31 |
| $D_{Fe^{2+}}$ | $0.72\times10^{-9}$ | $m^2/s$ | $Fe^{2+}$ | 32 |
| $D_{H^+}$ | $9.312\times10^{-9}$ | $m^2/s$ | $H^+$ | 31 |
| $D_{OH^-}$ | $5.26\times10^{-9}$ | $m^2/s$ | $OH^-$ | 31 |
| $D_{Fe(OH)^+}$ | $0.5\times10^{-9}$ | $m^2/s$ | $Fe(OH)^+$ | ## |
| $D_{O_2}$ | $1.96\times10^{-9}$ | $m^2/s$ | $O_2$ | 30 |
| **Standard potentials (vs. $Cu/CuSO_4$)** | | | | |
| $E_{Fe}^0$ | -0.756 | V | Iron oxidation | 29 |
| $E_{H_2O}^0$ (pH=14) | -1.144 | V | $H_2O$ reduction | 29 |
| $E_{H^+}^0$ (pH=0) | -0.316 | V | $H^+$ reduction | 29 |
| $E_{O_2}^0$ (pH=14) | 0.085 | V | $O_2$ reduction | 29 |
| **Number of electrons transferred** | | | | |


Copyright © 2010 by ASME

| | | | | |
|---|---|---|---|---|
| $n_{Fe}$ | 2 | | Iron oxidation | 33 |
| $n_{H_2O}$ | 1 | | $H_2O$ reduction | 29 |
| $n_{H^+}$ | 1 | | $H^+$ reduction | 29 |
| $n_{O_2}$ | 4 | | $O_2$ reduction | 33 |
| **Exchange current densities** | | | | |
| $i_{Fe}^{0}$ | 0.0002 | $A/m^2$ | Iron oxidation | 34-38 |
| $i_{H_2O}^{0}$ | 0.002 | $A/m^2$ | $H_2O$ reduction | 34 |
| $i_{H^+ref}^{0}$ | 0.002 | $A/m^2$ | $H_2O$ reduction | 34 |
| ($c_{H^+ref}$=0.1 $mol/m^3$) | | | | |
| $i_{O_2 Ref}^{0}$ | $4.0\times10^{-9}$ $A/m^2$ | | $O_2$ reduction | 33 |
| (pH=9, $p_{O_2\ ref}$ =1atm) | | | | |
| **Tafel slopes** | | | | |
| $b_{Fe}$ | 0.04 | V/decade | Iron oxidation | 30; 34 |
| $b_{H_2O}$ | 0.12 | V/decade | $H_2O$ reduction | 34 |
| $b_{H^+}$ | 0.12 | V/decade | $H^+$ reduction | 34 |
| $b_{O_2}$ (pH=9) | 0.12 | V/decade | $O_2$ reduction | 33 |

#: Based on parameters in OLI software;
##: Estimated.

**Table 3: Parameters and their Values Used for Switching On or Off One or More Conditions in the Modeling**

| No. | *Switch* | $\theta_1$ | $\theta_2$ | $\theta_3$ | $\theta_4$ | $D_{7c}$ |
|---|---|---|---|---|---|---|
| i | Constant gap vs. x and t, no current & no $O_2$ penetration via coating | 0 | 0 | 0 | 0 | 0 |
| ii | Variable gap vs. x (Fig.1b), no current & no $O_2$ penetration via coating | 1 | 0 | 0 | 0 | 0 |
| iii | Variable gap vs. x (Fig.1c), no current & no $O_2$ penetration via coating | 0 | 1 | 0 | 0 | 0 |
| iv | Variable gap vs. x (Fig.1b), no current but $O_2$ penetration via coating | 1 | 0 | 0 | 0 | 1 |
| v | Variable gap vs. x (Fig.1b), current but no $O_2$ penetration via coating | 1 | 0 | 1 | 0 | 0 |
| vi | Variable gap vs. x (Fig.1b), current and $O_2$ penetration via coating | 1 | 0 | 1 | 0 | 1 |
| vii | Variable gap vs. x (Fig.1b) <u>and vs. t</u>, no current and no $O_2$ penetration via coating | 1 | 0 | 0 | 1 | 0 |
| ix | Variable gap vs. x (Fig.1b) <u>and vs. t</u>, current and $O_2$ penetration via coating | 1 | 0 | 1 | 1 | 1 |

*where $\theta_1$ corresponds to variable gap vs. x shown by Figure 1b, $\theta_2$ to variable gap vs. x shown by Figure 1c (gap vs. x), $\theta_3$ to current penetration through coating, $\theta_4$ to variable gap vs. t due to metal loss at the steel surface, and m to $O_2$ penetration through coating.*


Copyright © 2010 by ASME

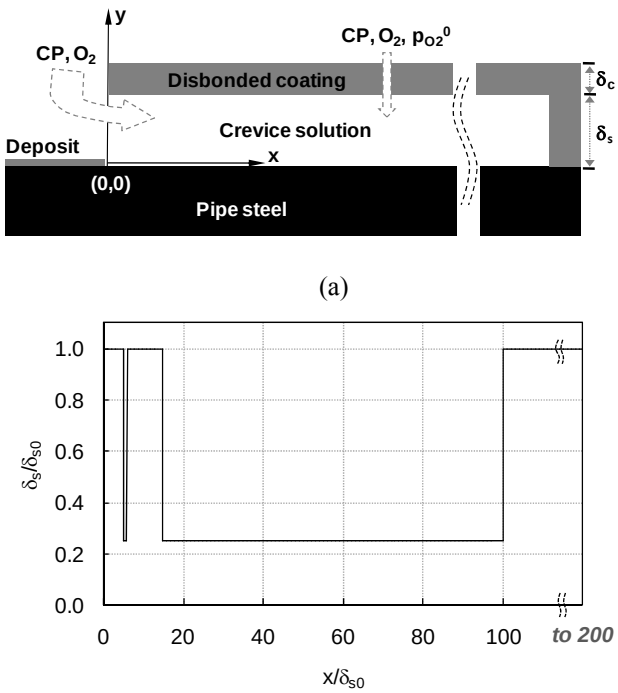


(a)




(b)

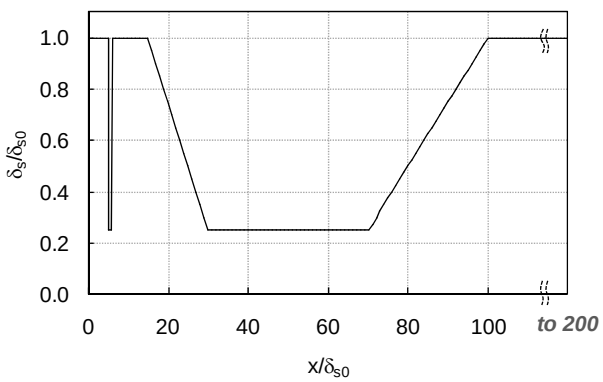


(c)

Figure 1. Model crevice geometry showing the coordinators and dimensions of the crevice and transport of CP current and $O_2$ into the crevice through the disbonded coating.

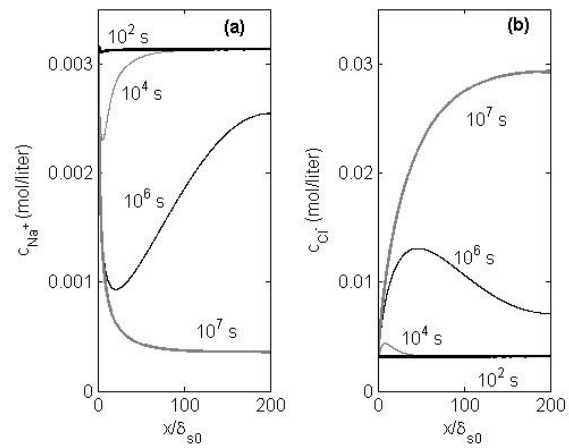


(a)

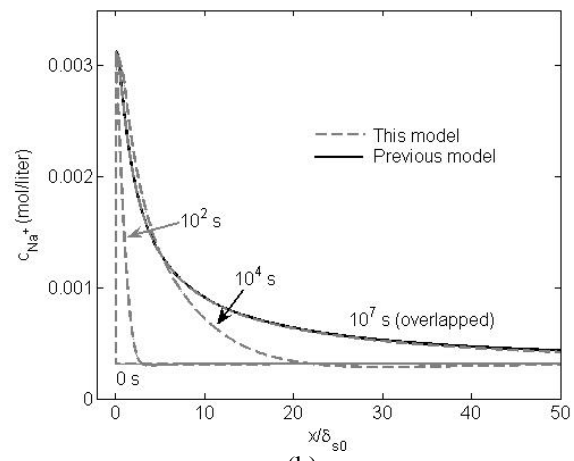


(b)

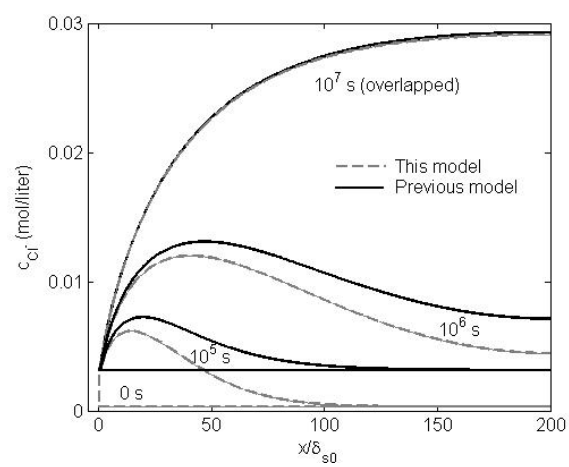


(c)

Figure 2. At a fixed mouth potential of -0.8071 $V_{CSE}$, with negligible or low initial CP, (a) evolution of $Na^+$ and $Cl^-$ concentrations with time in previous work with crevice Figure 1a where the initial and mouth chemistry are the same, (b) $Na^+$ concentration vs. time in this work with the initial concentrations different from the mouth concentrations of $Na^+$ and $Cl^-$ (gray lines), overlaying with the $Na^+$ concentration in previous work at $10^7$ s (dark line), and (c) similar to (b) but for $Cl^-$


Copyright © 2010 by ASME

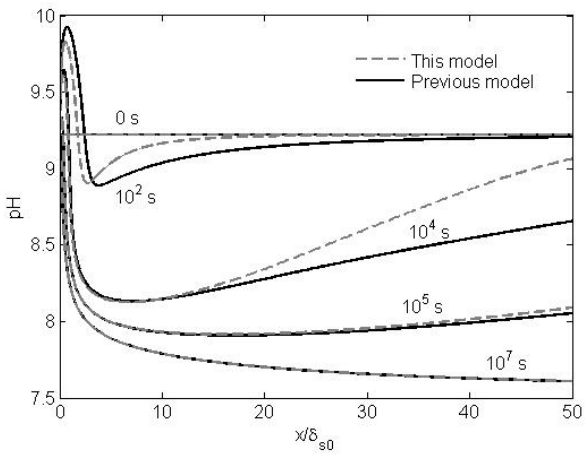


Figure 3. At a fixed mouth potential of -0.8071 $V_{CSE}$, with negligible or low initial CP, pH variation in crevice at different times; a comparison of the results obtained in this work with those in previous work.

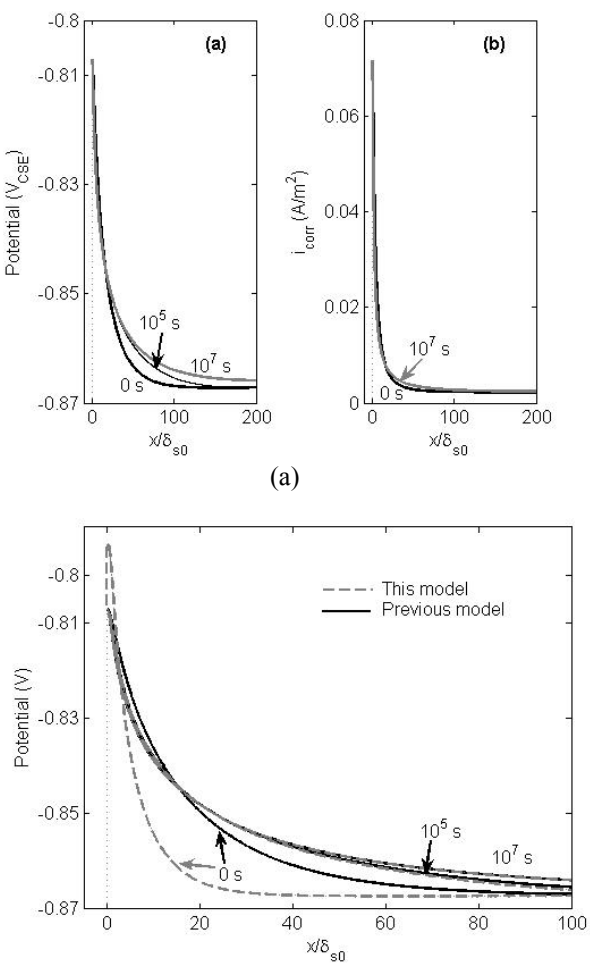


(a)

(b)

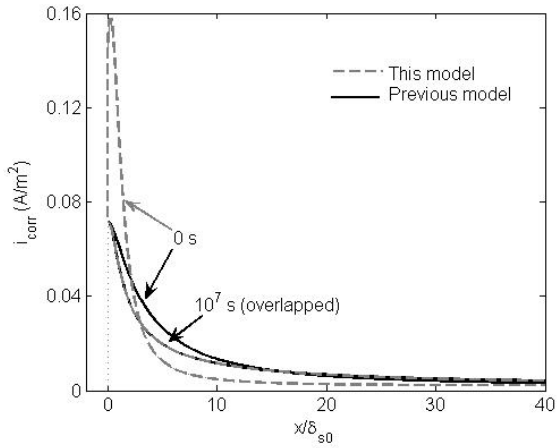


(c)

Figure 4. At a fixed mouth potential of -0.8071 $V_{CSE}$, with negligible or low initial CP, (a) variation of crevice potential and corrosion current density at different times obtained in previous work where the initial and mouth chemistry are the same, (b) variation of crevice potential at different times obtained in this work with the initial concentrations different from the mouth concentrations of $Na^+$ and $Cl^-$ (gray lines) in comparison with the potential in previous work at $10^7$ s (dark line), and (c) similar to (b) but with crevice corrosion current density.

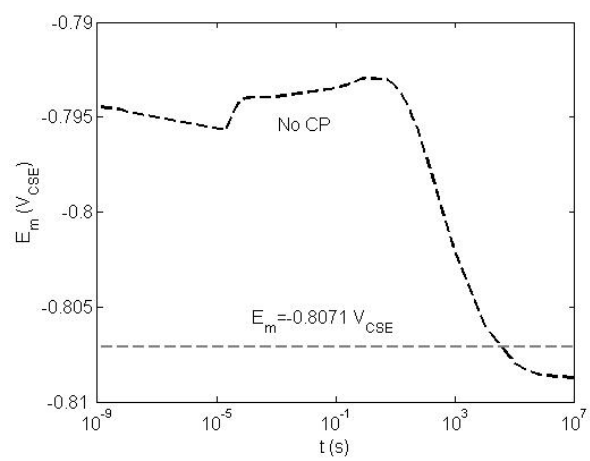


Figure 5. Variation of the crevice mouth potential with time during the corrosion process with no CP.


Copyright © 2010 by ASME

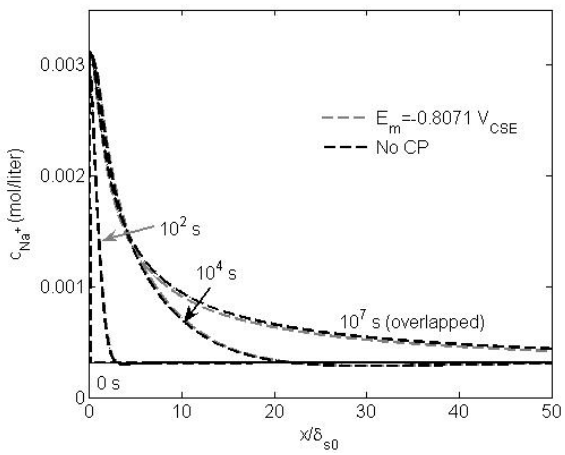


(a)

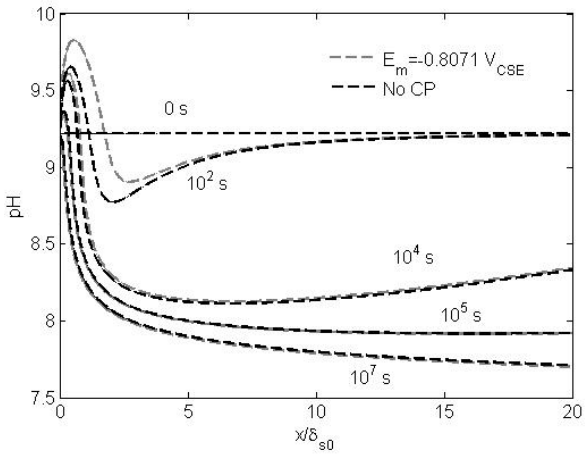


(b)

Figure 6. A comparison of: (a) $Na^+$ concentration and (b) pH in the crevice at different times between the crevice corrosion with no CP (dark lines) and low CP at a fixed potential of -0.8071 $V_{CSE}$ (gay lines).

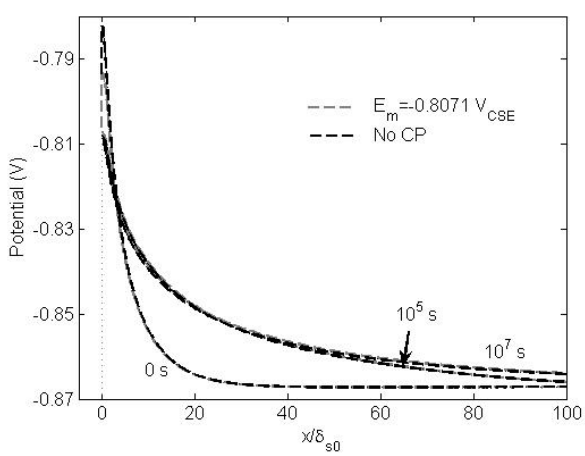


(a)

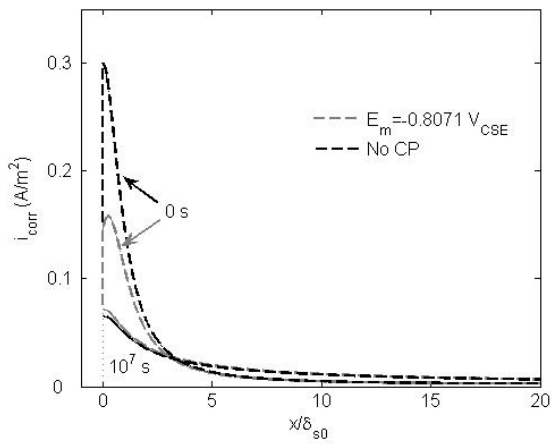


(b)

Figure 7. A comparison of: (a) potential and (b) corrosion current density in the crevice at different times between the crevice corrosion with no CP (dark lines) and low CP at a fixed potential of -0.8071 $V_{CSE}$ (gay lines).

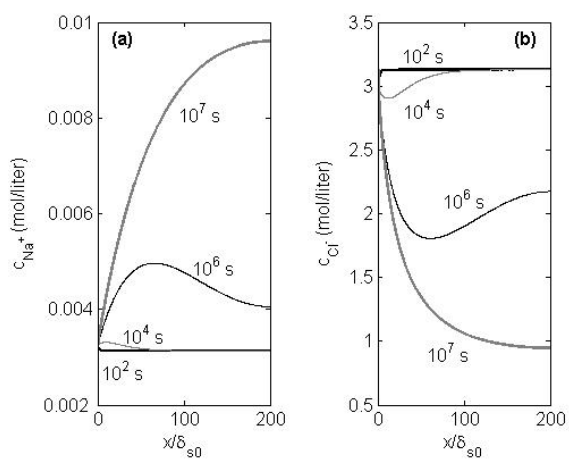


(a)

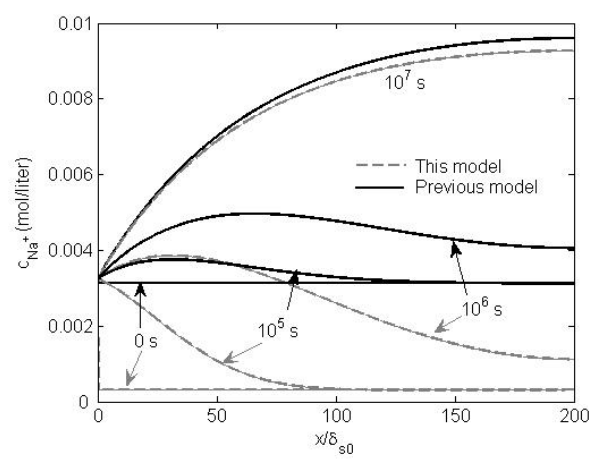


(b)

Figure 8. Similar to Figure 2, but here the mouth potential is fixed at -0.9 $V_{CSE}$.


Copyright © 2010 by ASME

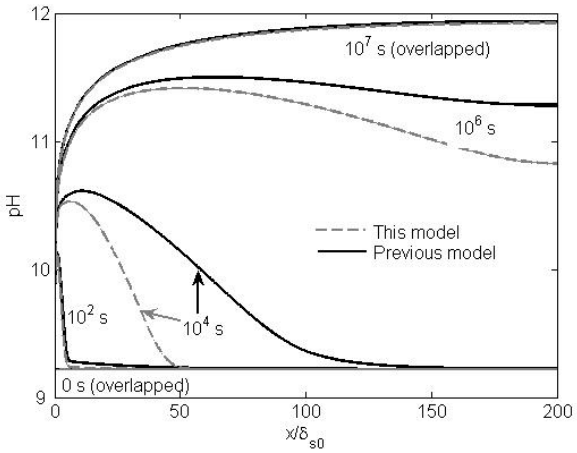


Figure 9. Similar to Figure 3, but here the mouth potential is fixed at -0.9 $V_{CSE}$.

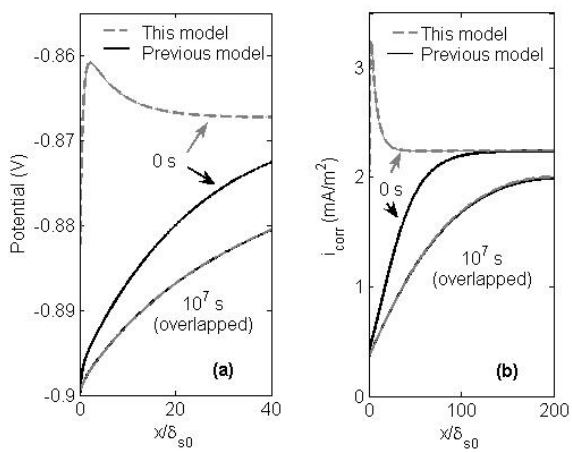


Figure 10. Similar to Figure 4, but here the mouth potential is fixed at -0.9 $V_{CSE}$.

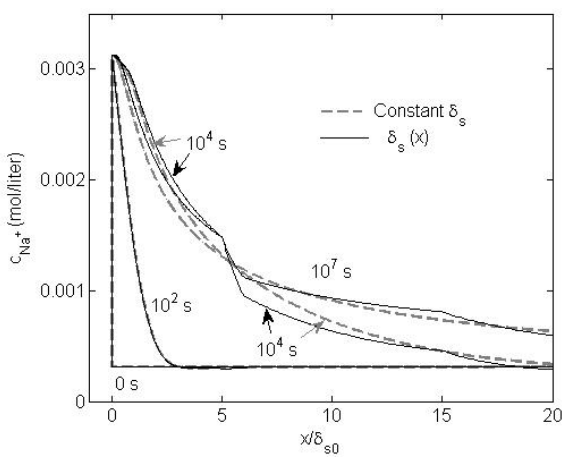


(a)

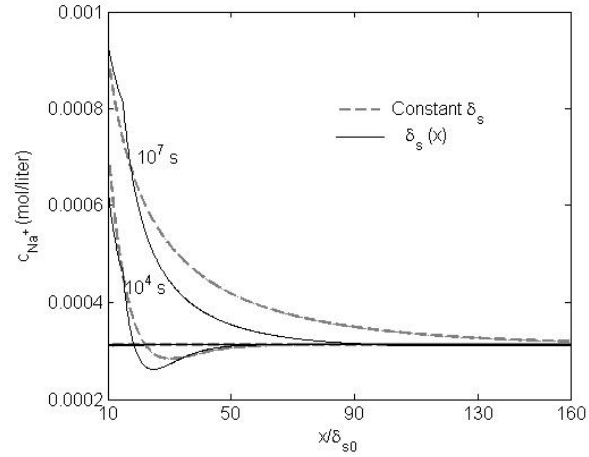


(b)

Figure 11. At a fixed mouth potential of -0.8071 $V_{CSE}$, a comparison of $Na^+$ concentrations in two crevices at different times between a constant gap shown by Figure 1a (gray lines) and variable gap vs. x shown by Figure 1b (gray lines): (a) near the mouth and (b) away from the crevice mouth.

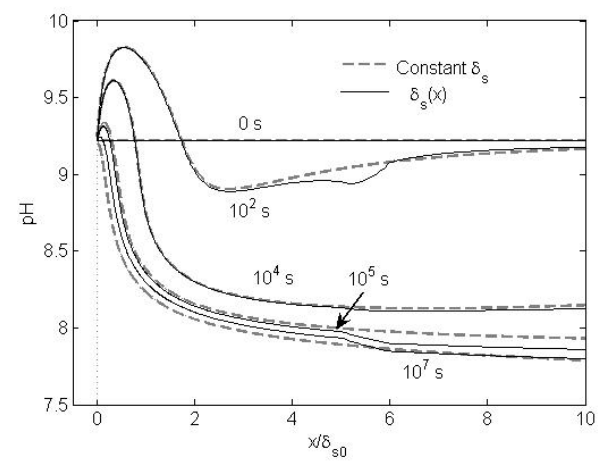


(a)

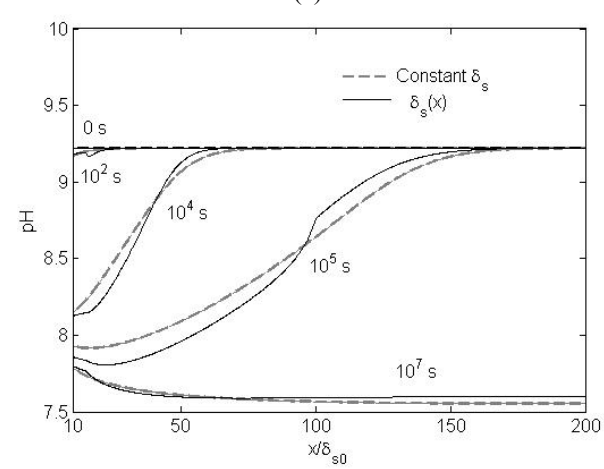


(b)

Figure 12. Similar to Figure 11 but here for a comparison of crevice pHs: (a) near the mouth and (b) away from the crevice


Copyright © 2010 by ASME

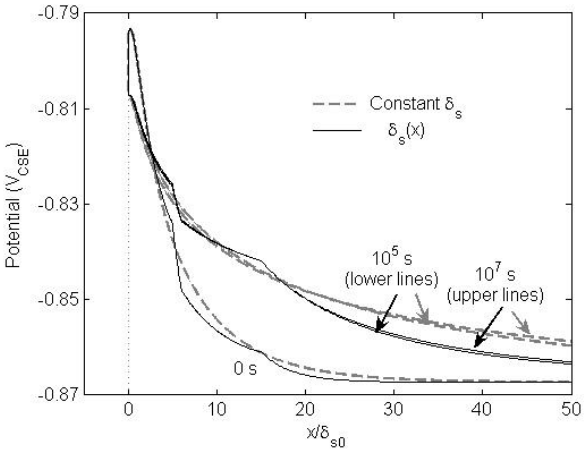


(a)

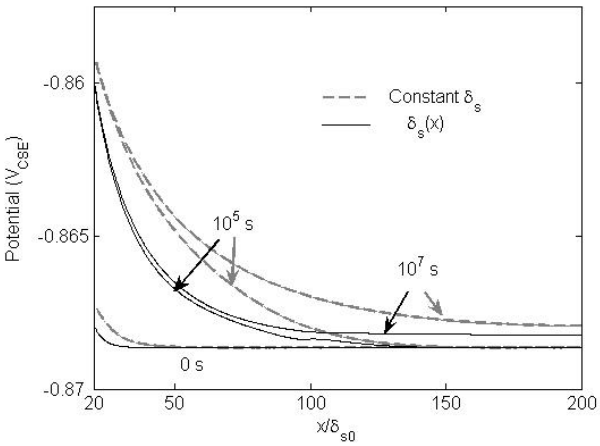


(b)

Figure 13. Similar to Figure 11 but here for a comparison of crevice potentials: (a) near the mouth and (b) away from the crevice mouth (note the reduced scale of potential from (a)).

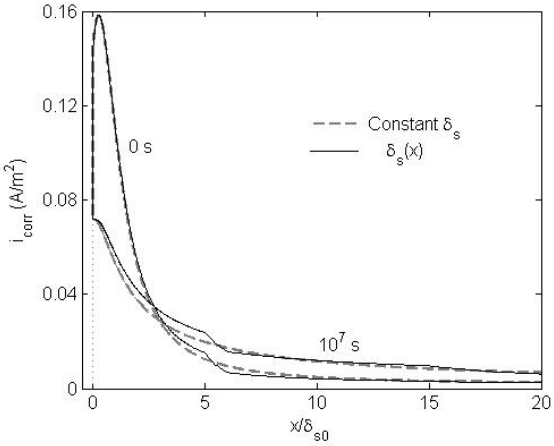


(a)

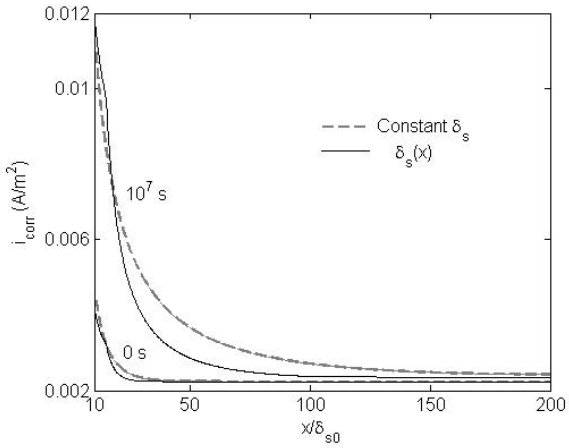


(b)

Figure 14. Similar to Figure 11 but here for a comparison of crevice corrosion current densities: (a) near the mouth and (b) away from the crevice mouth (note the reduced scale of $i_{corr}$ from (a)).

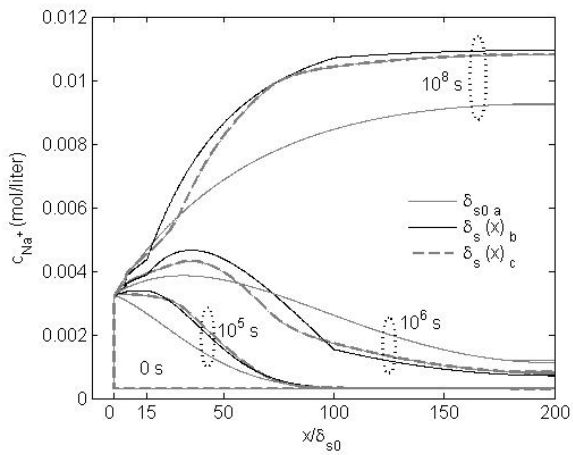


(a)

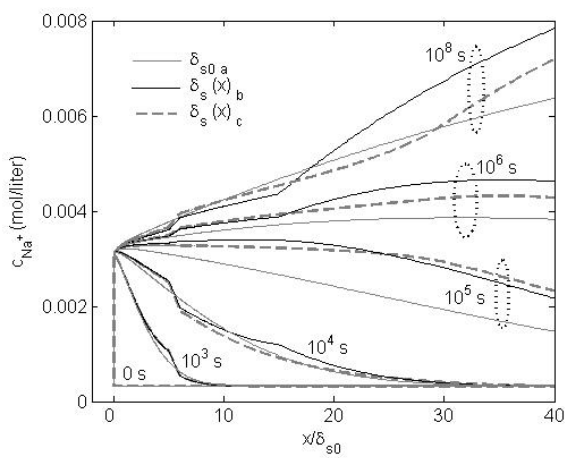


(b)

Figure 15. At a fixed mouth potential of -0.9 $V_{CSE}$, a comparison of $Na^+$ concentrations in the three crevices in Figure 1 at different times: constant gap of Figure 1a (gray solid lines), variable gap vs. x of Figure 1b (black solid lines), and variable gap vs. x of Figure 1c (gray broken lines): (a) the entire crevice and (b) near the mouth. In the legend, $\delta_{s0}$, $\delta_s(x)_b$ and $\delta_s(x)_c$ are referred to crevices shown in Figures 1a, b and c, respectively.


Copyright © 2010 by ASME

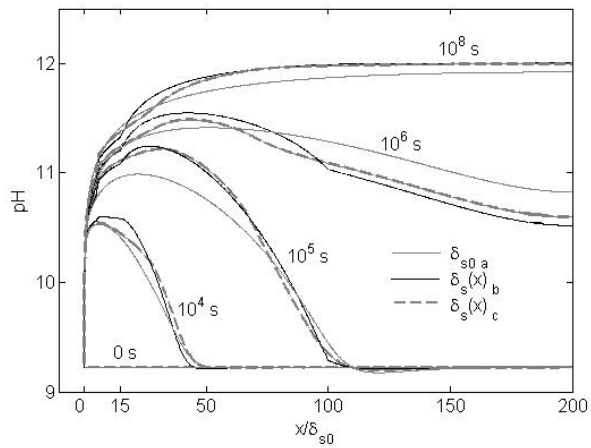


Figure 16.Similar to Figure 15 but here for a comparison of crevice pHs.

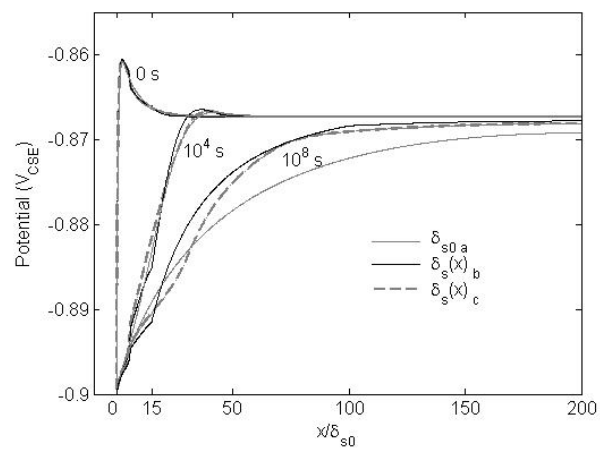


(a)

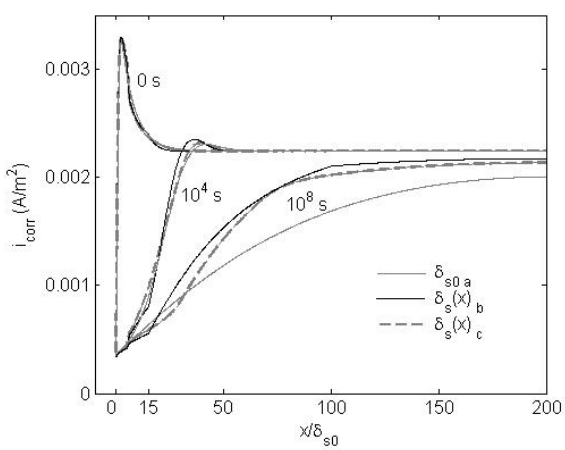


(b)

Figure 17. Similar to Figure 15 but here for a comparison of: (a) crevice potentials and (b) crevice corrosion current densities.


Copyright © 2010 by ASME